

Inverse flux quantum periodicity of magnetoresistance oscillations in two-dimensional short-period surface superlattices

X. F. Wang,[†] P. Vasilopoulos[◊], and F. M. Peeters^{*}

^{†,◊}*Concordia University Department of Physics*

1455 de Maisonneuve Ouest,

Montréal, Québec, Canada, H3G 1M8

^{*}*Departement Natuurkunde Universiteit Antwerpen (UIA),*

Universiteitsplein 1, B-2610, Belgium

(Dated: November 6, 2018)

Abstract

Transport properties of the two-dimensional electron gas (2DEG) are considered in the presence of a perpendicular magnetic field B and of a *weak* two-dimensional (2D) periodic potential modulation in the 2DEG plane. The symmetry of the latter is rectangular or hexagonal. The well-known solution of the corresponding tight-binding equation shows that each Landau level splits into several subbands when a rational number of flux quanta h/e pierces the unit cell and that the corresponding gaps are exponentially small. Assuming the latter are closed due to disorder gives analytical wave functions and simplifies considerably the evaluation of the magnetoresistivity tensor $\rho_{\mu\nu}$. The relative phase of the oscillations in ρ_{xx} and ρ_{yy} depends on the modulation periods involved. For a 2D modulation with a **short** period ≤ 100 nm, in addition to the Weiss oscillations the collisional contribution to the conductivity and consequently the tensor $\rho_{\mu\nu}$ show *prominent peaks when one flux quantum h/e passes through an integral number of unit cells* in good agreement with recent experiments. For periods 300 – 400 nm long used in early experiments, these peaks occur at fields 10 – 25 times smaller than those of the Weiss oscillations and are not resolved.

PACS numbers: 73.20.At; 73.20.Dx; 73.61.-r

I. INTRODUCTION

In the last decade the magnetotransport of the 2DEG, subjected to periodic potential modulations, has attracted considerable experimental [1] and theoretical [2, 3] attention. For one-dimensional (1D) modulations novel oscillations of the magnetoresistivity tensor $\rho_{\mu\nu}$ have been observed, at low magnetic fields B , distinctly different in period and temperature dependence from the usual Shubnikov-de Haas (SdH) ones observed at higher B . These novel oscillations reflect the commensurability between two length scales: the cyclotron diameter at the Fermi level $2R_c = 2\sqrt{2\pi n_e}\ell^2$, where n_e is the electron density, ℓ the magnetic length, and a the period of the potential modulation. The situation is similar but less clearcut for 2D modulations from both a theoretical [4]-[7] and an experimental [7, 9] point of view. To date most of the experimental results pertinent to 2D modulations [7]-[9] with square or hexagonal symmetry have indicated strongly that the predicted [10] fine structure of the Landau levels is not resolved. Magnetotransport theories pertinent to this case are rather limited [4],[7, 8] in contrast with those for 1D modulations.

Recent observations [9] call for additional theoretical work since they could not be fully explained by earlier semiclassical theories [4]. In this paper we develop, along the lines of Ref. 3, the relevant quantum mechanical magnetotransport theory of the 2DEG for precisely the case that the fine structure of the Landau levels is not resolved. Our goal is to explain recent experimental results [14] on 2D, short-period ($a \sim 1000\text{\AA}$) surface superlattices with mobility μ in the intermediate range, i.e., $\mu \sim 100 \text{ m}^2/\text{Vs}$. The symmetry of the 2D modulation is taken to be rectangular or hexagonal. A brief semiclassical account, pertinent to the former symmetry, was reported in Ref. 4 b). New magnetoresistance oscillations are found to occur *when one flux quantum h/e passes through an integral number of unit cells* as was recently observed experimentally [14]. Here we show that these oscillations result from the interplay between band conduction and collisional conduction. A new contribution to the latter opens up as hopping between cyclotron orbits which are separated by an integral multiple of the modulation period and have the same position relative to the modulation lattice. This contribution is appreciable only in short-period superlattices and accordingly could not be resolved in early experiments on long-period superlattices.

In the next section we derive the one-electron eigenfunctions and eigenvalues for rectangular and hexagonal modulations; we also present the density of states. The analytical and

numerical results for the corresponding conductivity or resistivity components are presented in Sec. III. Numerical results are given in Sec. IV and concluding remarks in Sec. V.

II. EIGENVECTORS, EIGENVALUES, AND DENSITY OF STATES

We consider a 2DEG, in the (x, y) plane, in the presence of a perpendicular magnetic field $\mathbf{B} = B\hat{z}$ and of a 2D periodic potential modulation $U(x, y)$. The electrons are considered as free particles with an effective mass m^* . In the absence of the modulation the normalized one-electron eigenfunction, in the gauge $\mathbf{A} = (0, Bx, 0)$, is given by $e^{ik_y y} \phi_n(x + x_0) / \sqrt{L_y}$ where $\phi_n(x + x_0)$ is the well-known harmonic oscillator function, centered at $-x_0 = -\ell^2 k_y$, and L_y is the sample's width.

In the presence of a sinusoidal 1D modulation one can use perturbation theory [2, 3] to evaluate the energy spectrum and eigenfunctions. Alternatively, one can use a tight-binding scheme, along the lines of Ref. [10], and look for solutions of the one-electron Hamiltonian $H^0 = (\mathbf{p} + e\mathbf{A})^2 / 2m^* + V_x \cos(K_x x)$ that are linear combinations of the unperturbed ($V_x = 0$) ones: $|\varphi_{nk_y}\rangle = \sum_p A_p |n, k_y + pG\rangle$, where G is a suitable wave vector introduced here for convenience and $|n, k_y + pG\rangle$ is the unperturbed state ($K_x = 2\pi/a_x$, and a_x is the modulation period along x). As in Ref. [10] we take $G \equiv K_y = 2\pi/a_y$ with a_y the modulation period along y . The summation over p has to be extended to all integer p values such that $-L_x/2\ell^2 \leq k_y + pK_y \leq L_x/2\ell^2$, where L_x is the length. For $p = 0$ we have the limits for k_y as $-a_x/2\ell^2 \leq k_y \leq a_x/2\ell^2$. Then the tight-binding equation $\langle n, k_y + pK_y | H^0 - E | \varphi_{nk_y} \rangle = 0$, in which mixing of different Landau levels n is neglected, gives acceptable solutions for the coefficients A_p as $A_p = A_0 \exp(i\xi p)$. The new states are labeled with the additional quantum number ξ ($0 \leq \xi \leq 2\pi$): $|\psi_{nk_y\xi}\rangle = A_0 \sum_p \exp(i\xi p) |n, k_y + pK_y\rangle$. The orthonormality condition $\langle \varphi_{nk_y\xi} | \varphi_{nk_y\xi'} \rangle = \delta_{\xi\xi'}$ gives $\xi = 2\pi\nu\ell^2 K_y / L_x \rightarrow k_x \ell^2 K_y$, ν being an integer, and $A_0 = \ell(K_y/L_x)^{1/2}$ by normalization. The energy spectrum obtained in this way is the same as that obtained by perturbation theory [2, 3].

We will now use this information to obtain the corresponding eigenvectors and eigenvalues for a 2D modulation potential.

A. Rectangular symmetry

We assume the following one-electron Hamiltonian

$$H^0 = (\mathbf{p} + e\mathbf{A})/2m^* + V_x \cos(K_x x) + V_y \cos(K_y y) \quad (1)$$

where $K_\mu = 2\pi/a_\mu$ ($\mu = x, y$); a_x and a_y are the periods along the x and y directions, respectively.

In the gauge chosen, $\mathbf{A} = (0, Bx, 0)$, the second term of Eq. (1) is not diagonal in k_y and therefore $|n, k_y\rangle$ is not a convenient basis set. But as in the 1D case we can look for solutions of Eq. (1) in the form $|\varphi_{n, k_y}\rangle = \sum_p A_p |n, k_y + pK_y\rangle$ as described above. This choice of eigenfunctions is also suggested by the fact that $V_y \cos K_y y$ connects the unperturbed state $|nk_y\rangle$ with only the states $|n, k_y \pm K_y\rangle$. In this case the equation $\langle n, k_y + pK_y | H^0 - E | \varphi_{n, k_y} \rangle = 0$, in which mixing of different Landau levels is neglected, takes the form

$$V_x F_n(u_x) \cos(2\pi p\alpha + K_x x_0) A_p + \frac{1}{2} V_y F_n(u_y) (A_{p+1} + A_{p-1}) = (E - E_n) A_p, \quad (2)$$

where $\alpha = 2\pi\ell^2/a_x a_y$, $E_n = (n + 1/2)\hbar\omega_c$ is the ‘‘unperturbed’’ eigenvalue and $\omega_c = |e|B/m^*$ the cyclotron frequency. Further, $F_n(u_\mu) = \exp(-u_\mu/2)L_n(u_\mu)$, $L_n(u_\mu)$ is the Laguerre polynomial, and $u_\mu = \ell^2 K_\mu^2/2$.

The solution of Eq. (2) gives the eigenvalues E and the eigenvectors A_p . We see immediately that for α integer the equation admits the exponential solutions $A_p = A_0 e^{i\xi p}$, with A_0 and ξ given above. This is also the case for those values of α for which $F_n(u_x)$ vanishes since $u_x = 2\pi^2\ell^2/a_x^2 = \pi(a_y/a_x)\alpha$. In the former case we have

$$E_{nk\xi} = E_n + V_x F_n(u_x) \cos(K_x x_0) + V_y F_n(u_y) \cos \xi \quad (3)$$

and in the latter

$$E_{nk\xi} = E_n + V_y F_n(u_y) \cos \xi, \quad (4)$$

where $\xi = (2\pi\nu/L_x)\ell^2 K_y \equiv \ell^2 K_y k_x$. In both cases the unperturbed Landau levels broaden into bands (with a bandwidth equal to $2(V_x|F_n(u_x)| + V_y|F_n(u_y)|)$ and $2V_y|F_n(u_y)|$, respectively), that oscillates with magnetic field B and (large) index n , cf. Refs. 2 and 3. The energy spectrum given by Eq. (3), plotted in Fig. 1 for $n = 0$, $\alpha = 1$, $V_x = 2V_y = 1$ meV, is a periodic function of k_x and of k_y since $\xi = \ell^2 K_y k_x$ and $x_0 = \ell^2 k_y$. Notice that the arguments of the cosines in Eq. (3) can be shifted by $2\pi\alpha$, α integer.

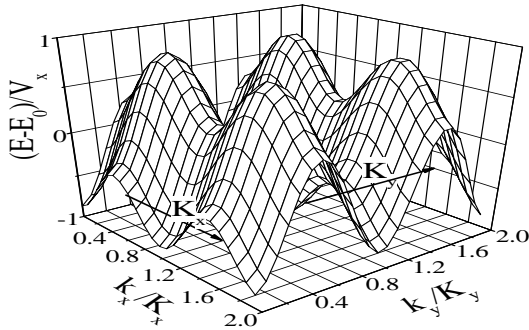


FIG. 1: Energy spectrum as a function of the wave vectors k_x and k_y for $n = 0$, $\alpha = 1$, $V_x = 2V_y = 1$ meV. The modulation wave vectors K_x and K_y are shown by the thick arrows.

One important consequence of this nonzero bandwidth is that the mean velocities v_x and v_y , which vanish in the absence of modulation, are now finite: from $v_\mu = dE_{nk\xi}/\hbar dk_\mu$, $\mu = x, y$, we obtain

$$v_x = -(\ell^2 K_y V_y / \hbar) F_n(u_y) \sin \xi, \quad (5)$$

and

$$v_y = -(\ell^2 K_x V_x / \hbar) F_n(u_x) \sin(K_x x_0). \quad (6)$$

Eqs. (5) and (6) lead to a finite diffusion or band conductivity which is absent when the modulation is not present, cf. Sec. II.

Equation (2) is the same as Harper's equation but the coefficients $V_\mu F_n(u_\mu)$ depend on the magnetic field. For B values other than those pertaining to Eq. (3) it has been shown by Hofstadter [11]a for the case of constant coefficients and by Claro and Wannier [11]b, for the case that the latter depend on B (hexagonal modulation), that the energy spectrum resulting from the numerical solution of Eq. (2), i.e., E , shows, when E is measured in units of $V_\mu F_n(u_\mu)$, a nontrivial structure: for $\alpha = i/j$, i, j being integers, each Landau level is split into j subbands and Eq. (2) is periodic with period j . Here, in view of the reported experiments [7]-[9] which did not indicate that this fine structure of the energy spectrum was resolved, we will assume that this is indeed the case, i.e., that in samples of not exceptionally high mobilities, such as those of Ref. 5, the small gaps mentioned above are closed due to disorder and justify the assumption below, see subsection C. That is, we assume that the Landau levels are bands. Now from the numerical solution of Eq. (2) we know that the bandwidth corresponding to $\alpha = i/j$ cannot exceed the value obtained from Eq. (3) or Eq. (4). Therefore, for computational convenience, we will assume that the energy spectrum is

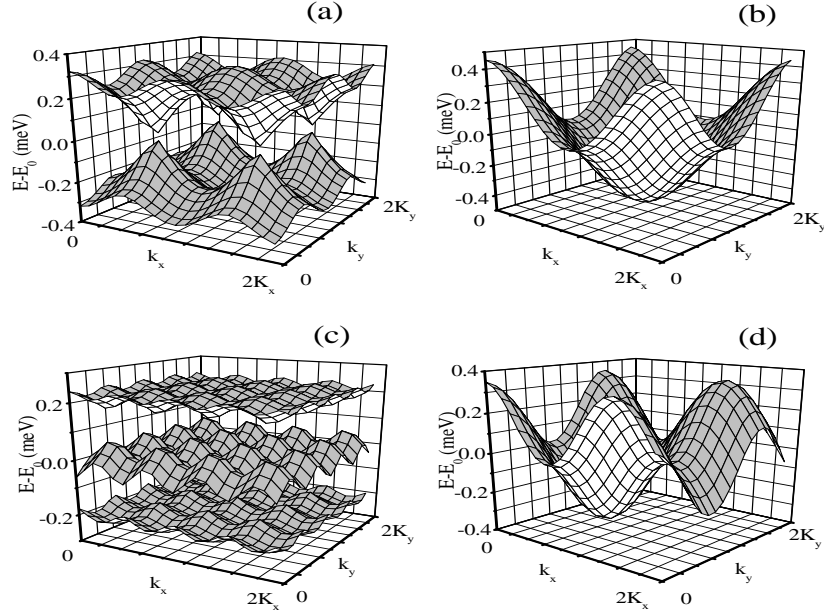


FIG. 2: Energy spectrum, obtained from the exact solution of Eq. (2), in (a) and (c), as a function of the wave vectors k_x and k_y for $n = 0$. The corresponding approximate spectrum, given by Eq. (3), is shown in (b) and (d). In (a) and (b) we have $\alpha = 1/2$ and $\alpha = 2/3$, in (c) and (d) $\alpha = 2/3$. The periods $a_x = a_y = 800\text{\AA}$ pertain to the experiment of Ref. [14].

given by Eq. (3) and the eigenfunctions by $|\psi_{nk_y\xi}\rangle = A_0 \sum_p e^{ip\xi} |n, k_y + pK_y\rangle$.

In Fig. 2 we compare the energy spectrum obtained by exactly solving Eq. (2) with the one given by Eq. (3). We do so because in the conductivity calculations we will use Eq. (3), as an approximation that will be justified, for all magnetic fields or values of α . The exact spectrum for $\alpha = i/j$ is composed of j minibands. Its dependence on k_x , which does not appear in Eq. (2), is obtained by introducing appropriate new basis states, in the manner of Ref. [12], with $|k_x| \leq \pi/ia_x$ and $|k_y| \leq \pi/a_y$ restricted in the magnetic Brillouin zone. As can be seen, the two spectra are quite different from each other. The corresponding difference in the density of states is much weaker if a small broadening is included, see subsection C below. For α integer, however, the exact spectrum and that given by Eq. (3) coincide; the result is shown in Fig. 1.

There are two alternative, *approximate* ways to obtain Eq. (3). First, we take $V_y \approx 0$

and use the corresponding 1D tight-binding states $|n, k_y, \xi\rangle$ to obtain the energy spectrum given by $E_n + V_x F_n(u_x) \cos(K_x x_0)$. We then use first-order perturbation theory, involving the states $|nk_y \xi\rangle$, to evaluate the energy correction to this spectrum due to the term $V_y \cos K_y y$ for $V_y \ll \hbar\omega_c + V_x$; the result is identical with that given by Eq. (3). Secondly, since these new oscillations of the magnetoresistance have been observed in weak magnetic fields and for weak modulations, we attempt a classical evaluation of the correction to the unperturbed energy E_n by the modulation $V_x \cos K_x x + V_y \cos K_y y$ using the classical equations of motion $x(t) = x_0 + R_c \sin(\omega_c t + \varphi)$, $y(t) = y_0 + R_c \cos(\omega_c t + \varphi)$; x_0 and y_0 are the classical center coordinates, R_c is the cyclotron radius, $\omega_c = |e|B/m^*$, and φ is a phase factor. Without loss of generality we may take $\varphi = 0$. Then, if T is the period of the cyclotron motion, a straightforward evaluation gives

$$\begin{aligned} \langle U \rangle &= (1/T) \int_{-T/2}^{T/2} dt [V_x \cos K_x x(t) + V_y \cos K_y y(t)] \\ &= V_x J_0(K_x R_c) \cos K_x x_0 + V_y J_0(K_y R_c) \cos K_y y_0, \end{aligned} \quad (7)$$

where $J_0(x)$ is the Bessel function of order zero. In the weak magnetic field limit $K_\mu R_c \gg 1$, Eq. (7) reduces to Eq. (3) for large n , i.e., for weak B . It is obvious that these three *approximate* ways of deriving the energy spectrum do not “see” its fine structure resulting from an exact numerical evaluation of the finite-difference Eq. (2) for $\alpha = i/j$. Therefore, they are applicable if the corresponding small gaps are closed due to disorder.

B. Hexagonal symmetry

We assume that the Hamiltonian is given by

$$H^0 = (\mathbf{p} + e\mathbf{A})^2/2m^* + V_x \cos K_x x \cos K_y y + V_y(1 + \cos 2K_y y)/2. \quad (8)$$

For $V_x = V_y = V_0$ this reduces to the model studied experimentally by Fang and Stiles [7]. If x and y are interchanged the energy spectrum, with $K_y = 2\pi/a$ and $K_x = 2\pi/\sqrt{3}a$, of the corresponding tight-binding equation has been studied numerically, for all values of the magnetic field, by Claro and Wannier [11] and has the same structure as that of the square symmetry. Here, in line with the case of rectangular symmetry, we assume that the small gaps of the energy spectrum are closed due to disorder and use again the tight-binding

description of Sec. II A. Corresponding to Eq. (2) we now obtain

$$\begin{aligned} \frac{1}{2}V_x F_n(u_x + u_y)[\cos(2\pi p\alpha + \gamma)A_{p+1} + \cos(2\pi p\alpha - \gamma)A_{p-1}] + \frac{V_y}{4}F_n(4u_y)[A_{p+2} + A_{p-2}] \\ = (E - E_n - \frac{1}{2}V_y)A_p, \end{aligned} \quad (9)$$

where $\gamma = K_x \ell^2(k_y + K_y/2)$. When α is integer Eq. (9) has the solution $A_p = A_0 \exp(i\xi p)$ with A_0 and ξ given in A and the eigenvalue E is given by

$$E_{nk\xi} = E_n + \frac{1}{2}V_y + V_x F_n(u_x + u_y) \cos \gamma \cos \xi + \frac{1}{2}V_y F_n(4u_y) \cos 2\xi, \quad (10)$$

where $\xi = \ell^2 K_y k_x$. We notice that for $K_x = 2\pi/a$ and $K_y = 2\pi\sqrt{3}a$, i.e. the usual hexagonal modulation, we have $F_n(u_x + u_y) = F_n(4u_y) = F_n(8\pi^2\ell^2/3a^2)$.

As in the rectangular case, we see that the Landau levels have broadened into bands with a bandwidth equal to $(2V_x|F_n(u_x + u_y) + V_y|F_n(4u_y)|)$ that oscillates with magnetic field and (large) n . Again the mean velocities v_x and v_y are finite

$$v_x = -(V_y \ell^2 K_y / \hbar) F_n(4u_y) \sin 2\xi - (V_x \ell^2 K_y / \hbar) F_n(u_x + u_y) \cos \gamma \cos \xi, \quad (11)$$

$$v_y = -(V_x \ell^2 K_x / \hbar) F_n(u_x + u_y) \sin \gamma \sin \xi; \quad (12)$$

this has important consequences for transport and will be detailed in the next section.

C. The density of states

The energy spectra given by Eqs. (3) and (10) are qualitatively different from the unmodulated spectrum, given by E_n , and from the corresponding 1D modulation spectrum given by $E_n + F_n(u_x) \cos K_x x_0$. These differences are also reflected in the density of states (DOS) defined by $D(E) = 2 \sum_{nk_y\xi} \delta(E - E_{nk_y\xi})$. For a 2D modulation with rectangular symmetry, corresponding to Eq. (3), the DOS becomes

$$D(E) = D_0 \sum_{n=0}^{\infty} \int_0^{2\pi} d\xi \{ [V_x F_n(u_x)]^2 - [E - E_n - V_y F_n(u_y) \cos \xi]^2 \}^{-1/2}, \quad (13)$$

while for the one with hexagonal symmetry, corresponding to Eq. (10), the DOS is given by

$$D(E) = D_0 \sum_{n=0}^{\infty} \int_0^{2\pi} d\xi \left\{ [V_x F_n(u_x + u_y) \cos \xi]^2 - \left(E - E_n - \frac{V_y}{2} [1 + F_n(4u_y) \cos 2\xi] \right)^2 \right\}^{-1/2}, \quad (14)$$

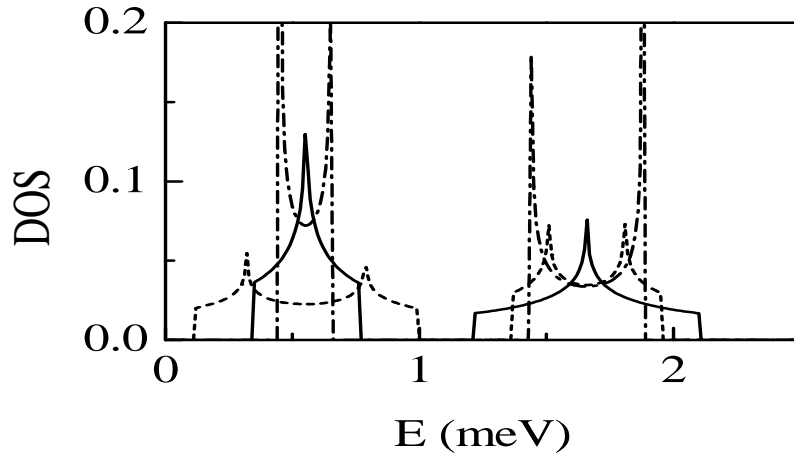


FIG. 3: Density of states versus energy for $V_x = V_y = 0.5$ meV, $a_x = 800$ Å with $a_y = 800$ Å and $a_y = 1600$ Å for the solid and dotted curves, respectively. The dash-dotted curve is the result for a 1D modulation along the x-direction with the same period and modulation strength as in the 2D case. The magnetic field is $B = 0.64$ T.

where $D_0 = L_y L_x / \pi^3 \ell^2$. The quantities within the curly brackets in Eqs. (13) and (14) must be positive.

In Fig. 3 we plot the DOS, given by Eq. (13), for various values of the parameters a_x , a_y , V_x , and V_y . For comparison we also show the DOS (dash-dotted curve) corresponding to the 1D modulation. The latter exhibits van Hove singularities at the edges of each Landau level (band) reflecting the 1D nature of the electron motion in this band, since $v_x \neq 0$ while $v_y = 0$, cf. Ref. 2 and 3. This is not the case for the 2D modulation: the electron motion is two-dimensional, since both v_x and v_y are different from zero, cf. Eqs. (5) and (6). That is, in the 2D case the DOS is finite, see also Ref. 4 b). As shown there, the DOS is qualitatively the same as the one shown in Fig. 3 if the periods are the same and the strengths are varied. This can be immediately deduced from the factors $V_x F_n(u_x)$ and $V_y F_n(u_y)$ that appear in Eqs. (3) and (11). The DOS for the hexagonal modulation is not shown since it's similar to the one shown in Fig. 3.

In Fig. 4 we compare the DOS obtained from the exact energy spectrum with that

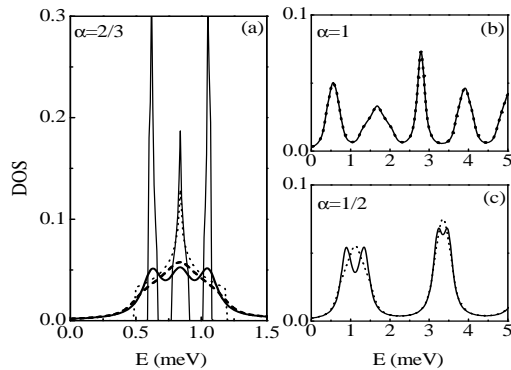


FIG. 4: (a) Density of states versus energy for $\alpha = 2/3$ and energy level width $\Gamma = 0$ (thin curves) and $\Gamma = 1K$ (thick curves). The solid and dotted curves are, respectively, the exact and approximate results. The DOS for $\alpha = 1$ in (b) and $\alpha = 1/2$ in (c) is plotted, respectively, for $\Gamma = 1.1K$ and $\Gamma = 1.5K$ obtained from $\Gamma = (e\hbar/m^*)\sqrt{B/\pi\mu}$. The parameters used are the same as those in Fig. 2.

obtained using Eq. (3). In this comparison we include a level broadening by replacing $\delta(E)$ in the definition of $D(E)$ by $\pi\Gamma/(E^2 + \Gamma^2)$. In Fig. 4(a) we show the influence of the level broadening on the DOS for $\alpha = 2/3$ and different values of Γ specified in the caption. As can be seen, the subband structure disappears with increasing Γ and the exact and approximate result approach each other. That is, the gaps between the minibands in each Landau level are closed with increasing level broadening. Notice that this happens for quite small values of Γ compared to the cyclotron energy which is about 1 meV in this example. As shown in (c), the same behavior of the DOS occurs for $\alpha = 1/2$. Notice also that this closeness between the exact and approximate DOS occurs despite the drastic difference in the corresponding energy spectra shown in Fig. 2. In addition, as shown in (b), for integer α the exact and approximate results for the DOS are identical.

III. TRANSPORT COEFFICIENTS

A. Basic expressions

For weak electric fields E , i.e. for linear responses, and weak scattering potentials the conductivity tensor $\sigma_{\mu\nu}(\omega)$ in the one-electron approximation, has been evaluated in detail in Ref. 3: $\sigma_{\mu\nu}(\omega) = \sigma_{\mu\nu}^d(\omega) + \sigma_{\mu\nu}^{nd}(\omega)$, $\mu, \nu = x, y$. The contribution $\sigma_{\mu\nu}^d(\omega)$ stems from the diagonal part of the density operator ρ . In a suitable basis $\langle J_\mu^d \rangle = \text{Tr}(\rho^d J_\mu) = \sigma_{\mu\nu}^d E_\nu$, where J_μ is the current density, and $\sigma_{\mu\nu}^{nd}(\omega)$ comes from the nondiagonal part of ρ ($\rho = \rho^d + \rho^{nd}$). In general $\sigma_{\mu\nu}^d(\omega) = \sigma_{\mu\nu}^{dif}(\omega) + \sigma_{\mu\nu}^{col}(\omega)$, where $\sigma_{\mu\nu}^{dif}(\omega)$ indicates diffusive contributions and $\sigma_{\mu\nu}^{col}(\omega)$ collisional contributions. For the diffusive contribution we have

$$\sigma_{\mu\nu}^{dif}(0) = \frac{\beta e^2}{\Omega} \sum_{\zeta} f_{\zeta}(1 - f_{\zeta}) \tau(E_{\zeta}) v_{\mu}^{\zeta} v_{\nu}^{\zeta}, \quad (15)$$

provided that the scattering is elastic or quasielastic, and for the collisional one

$$\sigma_{\mu\nu}^{col}(0) = \frac{e^2}{2\Omega} \sum_{\zeta\zeta'} f_{\zeta}(1 - f_{\zeta'}) W_{\zeta\zeta'} (\alpha_{\mu}^{\zeta} - \alpha_{\mu}^{\zeta'})^2, \quad (16)$$

for both elastic ($f_{\zeta} = f_{\zeta'}$) and inelastic ($f_{\zeta} \neq f_{\zeta'}$) scattering. $W_{\zeta\zeta'}$ is the transition rate between the unperturbed one-electron states $|\zeta\rangle$ and $|\zeta'\rangle$, Ω the volume of the system, e the electron charge, $\tau(E_{\zeta})$ the relaxation time, and $\alpha_{\mu}^{\zeta} = \langle \zeta | r_{\mu} | \zeta \rangle$ the mean value of the μ -component of the position operator when the electron is in state $|\zeta\rangle$ and has velocity $v_{\mu}^{\zeta} = \langle \zeta | v_{\mu} | \zeta \rangle$. Equation (15) describes transport through extended states whereas Eq. (16) deals with transport through localized states and is absent in semiclassical treatments.

The nondiagonal contribution $\sigma_{\mu\nu}^{nd}(\omega)$ to the conductivity is given by

$$\begin{aligned} \sigma_{\mu\nu}^{nd}(\omega) = & \frac{2i\hbar e^2}{\Omega} \sum_{\zeta \neq \zeta'} f_{\zeta}(1 - f_{\zeta'}) \langle \zeta | v_{\mu} | \zeta' \rangle \langle \zeta' | v_{\nu} | \zeta \rangle \\ & \times \frac{1 - e^{\beta(E_{\zeta} - E_{\zeta'})}}{E_{\zeta} - E_{\zeta'}} \lim_{\epsilon \rightarrow 0} \frac{1}{E_{\zeta} - E_{\zeta'} + \hbar\omega + i\epsilon}. \end{aligned} \quad (17)$$

If we use the identity $f_{\zeta}(1 - f_{\zeta'}) \exp[\beta(E_{\zeta} - E_{\zeta'})] = f_{\zeta'}(1 - f_{\zeta})$, Eq. (17) takes the form of the well-known Kubo-Greenwood formula.

Apart from their use in Ref. 3 for the 1D modulation case, the above formulas have also been successfully applied to various situations of electronic transport, such as hopping conduction [13]a, Aharonov-Bohm effect [13]b, quantum Hall effect [13]c, etc.

The resistivity tensor $\rho_{\mu\nu}$ is given in terms of the conductivity tensor $\rho = \sigma^{-1}$. We will use the standard expressions $\rho_{xx} = \sigma_{yy}/S$, $\rho_{yy} = \sigma_{xx}/S$, and $\rho_{yx} = -\rho_{xy} = -\sigma_{yx}/S$ with $S = \sigma_{xx}\sigma_{yy} - \sigma_{xy}\sigma_{yx}$.

B. Analytical evaluations

The scattering mechanism enters the conductivity expressions (15) and (16) through the relaxation time $\tau(E_\zeta)$ and the transition rate $W_{\zeta\zeta'}$, respectively; in contrast, Eq. (17) is independent of the scattering when the latter is weak [13].

We assume that the electrons are scattered elastically by randomly distributed impurities. This type of scattering is dominant at the low temperatures of the reported experiments. Further, we expand the impurity potential in Fourier components, i.e., $U(\mathbf{r} - \mathbf{R}) = \sum_{\mathbf{q}} U_{\mathbf{q}} \exp[i\mathbf{q}\cdot(\mathbf{r} - \mathbf{R})]$, with $U_{\mathbf{q}} = 2\pi e^2/\epsilon(q^2 + k_s^2)^{1/2}$ corresponding to the screened impurity potential $U(\mathbf{r}) = (e^2/\epsilon r) \exp(-k_s r)$; \mathbf{r} and \mathbf{R} are the electron and impurity positions, respectively, $\mathbf{q} = q_x \hat{x} + q_y \hat{y}$, ϵ is the dielectric constant, and k_s the screening wave vector.

Diffusive contribution. For weak modulation potentials V_x and V_y , which is pertinent to most of the reported experiments, we may use $|\zeta\rangle = |n, k_y, \xi\rangle$ to evaluate the velocity matrix elements appearing in Eq. (15); the latter are given by Eqs. (5) and (6) for *rectangular* symmetry and by Eqs. (11) and (12) for *hexagonal* symmetry. As for the relaxation time $\tau(E_\zeta)$, it is defined by $1/\tau(E_\zeta) = \sum_{\zeta'} W_{\zeta\zeta'}(v_\zeta - v'_{\zeta'})/v_\zeta$. Though the Landau levels broaden into bands, this definition fails at the flat-band conditions, when $v_\zeta = v'_{\zeta'} = 0$. For this reason we estimate it from the lifetime given by $1/\tau(E_\zeta) = \sum_{\zeta'} W_{\zeta\zeta'}$. In the limit $k_s \gg q$, we obtain $\tau = \tau(E_\zeta) \approx (\pi\ell^2\hbar^2/N_I U_0^2)^{1/2}$ where N_I is the 2D impurity density and $U_0 \approx 2\pi e^2/\epsilon k_s$. However, at weak magnetic fields we may use τ as constant and estimate it from the zero-field mobility μ : $\tau = \tau_0 = \mu m^*/e$.

We now use Eqs. (5), (6), and (15) with $\sum_k \rightarrow (L_y/\pi) \int_0^{a_x/2\ell^2} dk_y$ and $\sum_\xi \rightarrow (L_x/\pi a_x) \int_0^{2\pi} d\xi$. The result for σ_{xx}^{dif} is

$$\sigma_{xx}^{dif} \approx \frac{e^2}{h} \frac{\beta\tau}{\hbar\pi a_x} K_y^2 \ell^4 V_y^2 \sum_n e^{-u_y} [L_n(u_y)]^2 \int_0^{2\pi} d\xi \int_0^{a_x/\ell^2} dk_y f_{nk_y\xi} (1 - f_{nk_y\xi}) \sin^2 \xi. \quad (18)$$

The component σ_{yy}^{dif} is given by Eq. (18) with x and y interchanged, and $\sin^2 \xi$ replaced by $\sin^2(\ell^2 K_x k_y) = \sin^2(K_x x_0)$. In the limit of vanishing V_y Eq. (18) gives the result of

a 1D modulation, $\sigma_{xx}^{dif} = 0$. If we neglect the weak k_y - and ξ -dependence of the factor $f_{nk_y\xi}(1 - f_{nk_y\xi})$ we obtain the simplified expression

$$\sigma_{xx}^{dif} \approx \frac{e^2}{h} \frac{\beta\tau}{\hbar} K_y^2 \ell^2 V_y^2 \sum_n e^{-u_y} [L_n(u_y)]^2 f_n(1 - f_n). \quad (19)$$

The corresponding expression for σ_{yy}^{dif} is given by Eq. (19) with x and y interchanged.

For *hexagonal* symmetry we use $K_x = 2\pi/a$ and $K_y = 2\pi/\sqrt{3}a$. The results for σ_{xx}^{dif} and σ_{yy}^{dif} are similar to Eq. (18) and can be easily obtained using Eqs. (11) and (12) for the velocities. The result for σ_{yy}^{dif} , corresponding to Eq. (19), is given by Eq. (19) with $K_y^2 V_y^2$ replaced by $K_x^2 V_x^2/2$ and that for σ_{xx}^{dif} by

$$\sigma_{xx}^{dif} \approx \pi \frac{e^2}{h} \frac{\beta\tau}{\hbar} K_y^2 V_y^2 \left(1 + \frac{V_x^2}{2V_y^2}\right) e^{-u} \sum_n [L_n(u)]^2 f_n(1 - f_n), \quad (20)$$

where $u = 8\pi^2 \ell^2/3a^2$.

Collisional contribution. To evaluate this contribution to order V_μ^2 we must use the perturbed wave function to order V_μ . The procedure for evaluating Eq. (16) is identical with that corresponding to the 1D modulation detailed previously [3]. We have again $\langle \zeta | x | \zeta \rangle - \langle \zeta' | x | \zeta' \rangle = \ell^2(k_y - k'_y)$; the only new ingredient are the following matrix elements

$$\langle nk_y\xi | y | nk_y\xi \rangle = -\xi/K_y \quad (21)$$

and

$$|\langle nk_y\xi | e^{i\mathbf{q}\cdot\mathbf{r}} | n'k'_y\xi' \rangle|^2 = (n!/n')! u^{n'-n} e^{-u} \left[L_n^{n'-n}(u) \right]^2 \delta_{\xi,\xi'+c_y q_x} \delta_{k_y,k'_y-q_y}, \quad (22)$$

where $u = \ell^2(q_x^2 + q_y^2)/2$ and $c_y = \ell^2 K_y$.

We now use Eqs. (16), (20)-(21), and the standard expression for the transition rate

$$W_{\zeta\zeta'} = \sum_{\mathbf{q}} U_{\mathbf{q}}^2 |\langle nk_y\xi | e^{i\mathbf{q}\cdot\mathbf{r}} | n'k'_y\xi' \rangle|^2 \delta(E_{nk_y\xi} - E_{n'k'_y\xi'}). \quad (23)$$

We use the spectrum (3) and shift the argument of the cosines by $\ell^2 K_x K_y = 2\pi\alpha$, α integer, in the δ function as well as in the factor $f_{nk_y\xi}(1 - f_{n'k'_y\xi'})$. Then Eq. (16) takes the form

$$\begin{aligned} \sigma_{yy}^{col} &\approx \frac{e^2}{h} \frac{\beta N_I U_0^2}{4a_x} \sum_{n,n'} \int_0^\infty du e^{-u} u^{n'-n+1} [L_n^{n'-n}(u)]^2 \\ &\times \int_0^{2\pi} d\xi \int_0^{a_x/\ell^2} dk_y f_{nk_y\xi}(1 - f_{n',k_y+K_y+q_y,\xi-c_y(K_x+q_x)}) \\ &\times \delta(E_{nk_y\xi} - E_{n',k_y+K_y+q_y,\xi-c_y(K_x+q_x)}). \end{aligned} \quad (24)$$

We proceed as follows. For weak magnetic fields involved in the problem the Landau-level index n is large and the major contributions to the sum over n' come from n' values close n . With the asymptotic expansion of the Laguerre polynomials, $e^{-u/2}L_n(u) \approx (\pi^2 nu)^{-1/4} \cos(2\sqrt{nu} - \pi/4)$, it's an excellent approximation to take $F_n(u_\mu) \approx F_{n'}(u_\mu)$. Then the δ function becomes

$$\begin{aligned} \delta(E_{nk_y\xi} - E_{n',k_y+K_y+q_y,\xi-c_y(K_x+q_x)}) &\approx \delta[(n - n')\hbar\omega_c \\ &+ 2F_n(u_x)V_x \sin c_x(K_y - q_y/2) \sin c_x(k_y + K_y - q_y/2) \\ &+ 2F_n(u_y)V_y \sin c_y(K_x - q_x/2) \sin c_y(k_x + K_x - q_x/2)]. \end{aligned} \quad (25)$$

The shift by $\ell^2 K_x K_y = 2\pi\alpha$, α integer, in Eq. (25) and in the factor $f_{nk_y\xi}(1 - f_{n'k'_y\xi'})$ was made to stress the formal validity of Eqs. (24) and (25) for α integer. If we don't make it, we must put $K_x = K_y = 0$ in the sine factors and change $E_{n',k_y+K_y+q_y,\xi-c_y(K_x+q_x)}$ to $E_{n',k_y+q_y,\xi-c_y q_x}$ wherever it appears. For α close to an integer though, one can reinstate K_x and K_y in Eqs. (24) and (25) as shown.

We now remark that the largest contribution to the integral over u in Eq. (24) comes from very small values of q_x and q_y due to the factor $\exp(-u)$ or the factor $1/\sqrt{\pi^2 nu}$ in the asymptotic expression $e^{-u}[L_n(u)]^2 \approx \cos^2(2\sqrt{nu} - \pi/4)/\sqrt{\pi^2 nu}$. In addition, for the usual 2D systems we have $k_s \approx 10^8/\text{m}$ which is much larger than these small values of q_x and q_y . With that in mind and in order to reduce the numerical work, we replace the δ function (25) by a Lorentzian of width Γ and neglect in it and in the factor $f_{nk_y\xi}(1 - f_{n',k_y+K_y+q_y,\xi-c_y(K_x+q_x)})$ the terms $\propto q_x$ or $\propto q_y$. Alternatively, we may expand the δ function in powers of q_x and q_y ; then by far the leading contribution comes from the zero-order term given by Eq. (25) with $q_x = q_y = 0$. In addition, we neglect the term q^2 in $U_{\mathbf{q}}$. Further, from the sum over n' we consider only the terms $n' = n$ and $n' = n \pm 1$; the term $n' = n$ gives the dominant contribution, about 90%. Then the integral over u can be evaluated and Eq. (24) takes the form

$$\begin{aligned} \sigma_{yy}^{col} &\approx \frac{e^2 \beta N_I U_0^2 \Gamma}{h 2\pi^2 a_x} \sum_n \{(2n + 1) \int_0^{2\pi} d\xi \int_0^{a_x/\ell^2} dk_y \\ &\times [D_{n,n} + (n + 1)D_{n,n+1} + nD_{n,n-1}]\} \end{aligned} \quad (26)$$

where

$$D_{n,n'} = f_{nk_y\xi}(1 - f_{n',k_y+K_y,\xi-c_y K_x}) / [(E_{nk_y\xi} - E_{n',k_y+K_y,\xi-c_y K_x})^2 + \Gamma^2] \quad (27)$$

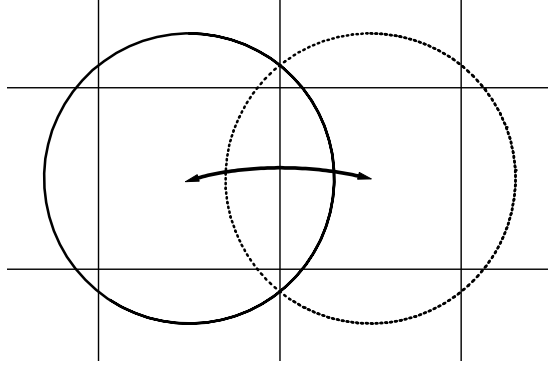


FIG. 5: Scattering between two cyclotron orbits which encircle one unit cell.

As a result, when $2\pi\ell^2/a_x a_y = \Phi_0/\Phi$ is an integer, the second and third terms in the argument of the δ function in Eq. (25) vanish and entail $n = n'$, i. e., *the response is strongest when one flux quantum passes through an integral number of cells* as observed [8, 14]. In this case the factor $[(\dots)^2 + \Gamma^2]$ in Eq. (27) becomes Γ^2 .

A qualitative understanding of the enhancement of the collisional conductivity for integer $\alpha = \Phi_0/\Phi$ is as follows. In this case only scattering between the states $|k_y, \xi\rangle$ and $|k_y + K_y + q_y, \xi + cy(K_x, q_x)\rangle$ is allowed, cf. Eq. (24). These states correspond to cyclotron orbits separated by a distance αa_x which is a multiple of the lattice period. One example is shown in Fig. 5 for two orbits that encircle a unit cell. As shown, the orbits are in the same relative position with respect to the modulation lattice and correspond to electron states of the same energy. Since impurity scattering is an elastic process that leads to hopping between states of the same energy, the hopping between such cyclotron orbits for integer α contributes the most to the conduction and enhances the collisional conductivity. On the other hand, for α not an integer the position of the two orbits involved in the scattering process relative to the modulation lattice changes; accordingly the enhancement mentioned above is weakened.

For those values of the magnetic field for which $F_n(u_x)$ vanishes we use the same wave functions and the spectrum (4). If the modulation periods are the same, we have $F_n(u_x) = F_n(u_y) = 0$, $n \rightarrow n'$, and Eq. (26) holds with $D_{n,n\pm 1} \rightarrow 0$. If the modulation periods are

not equal or if Φ_0/Φ is not an integer, Eqs. (25) and (26) hold only approximately. With all that in mind, the assumption that the small gaps are closed due to disorder, and for computational convenience, we use Eq. (26) as an approximation for all fields.

For the *hexagonal* modulation we obtain again Eq. (26) but now the energy spectrum is given by Eq. (10). Further, a_x and u_y are replaced by a and $u = 8n^2\ell^2/3a^2$, respectively. For σ_{xx}^{col} the result is given by Eq. (26) with a_x replaced by a ; u remains the same.

The Hall conductivity. The evaluation of Eq. (17) for $\omega = 0$ is readily performed with the states $|nk_y\xi\rangle$ and the energy levels given by Eqs. (3) or (10). The only difference with the previous [3] calculation is that a factor $\exp[i(k_y - k'_y)/K_y]\delta_{\xi,\xi'}$ appears on the rhs of Eq. (17) of Ref. 3 now written as $\langle nk_y\xi | V_\mu | n'k'_y\xi' \rangle$. For *rectangular* symmetry we obtain ($\sigma_{yx}(0) \equiv \sigma_{yx}$)

$$\sigma_{yx} = \frac{e^2}{h} \frac{2\ell^2}{\pi a_x} \sum_n (2n+1) \int_0^{a_x/2\ell^2} dk_y \int_0^{2\pi} d\xi \frac{f_{nk_y\xi} - f_{n+1,k_y\xi}}{[1 + \lambda_{nx} \cos(K_x x_0) + \lambda_{ny} \cos \xi]^2}, \quad (28)$$

where $\lambda_{n\mu} = V_\mu e^{-u_\mu/2} L_{n+1}^{-1}(u_\mu)/\hbar\omega_c$, $\mu = x, y$. We notice that for $V_y = 0$ we obtain the previous 1D result [3]. We also remark that Eq. (28) is valid for hexagonal symmetry with $a_x \rightarrow a$, $u_x = u_y = u = 8\pi^2\ell^2/3a^2$ and of course the different energy levels (Eq. (10)) that enter the factor $f_{nk_y\xi}$.

IV. NUMERICAL RESULTS

We now present results for the various resistivity components $\rho_{\mu\nu}$ using the standard expressions given at the end of Sec. III. A, and evaluating numerically the conductivities given by Eqs. (18), (26), and (27). For Figs. 3-7, and 10 we use the parameters of Ref. 8. They are: electron density $n_s = 4.5 \times 10^{15}/m^2$, temperature $T = 5.5$ K or $T = 1.6$ K, $a_x = a_y = 804\text{\AA}$, and mobility $\mu = 70 m^2/Vs$. The corresponding parameters for Figs. 8-9, taken from Ref. 5, are $n_s = 5.1 \times 10^{15}/m^2$, temperature $T = 4.2$ K, $a_x = a_y = 2820\text{\AA}$, and mobility $\mu = 140 m^2/Vs$. The relaxation time at zero magnetic field τ_0 is estimated from the sample mobility as $\tau_0 = m^*\mu/e$. Then the level width is $\Gamma = (eBN_I U_0^2/\pi\hbar)^{1/2} = (e\hbar/m^*)\sqrt{B/\pi\mu}$.

In Figs. 3 we plot ρ_{xx} and ρ_{yy} as function of the magnetic field B with $V_x = 0.5$ meV for constant $\tau = \tau_0$. As indicated, the various curves correspond to different V_y and the dotted one, marked 1D, represents the 1D limit obtained with $V_y = 0$. The prominent peaks in the 2D case, marked by the integral value of α , result from the collisional contribution to the con-

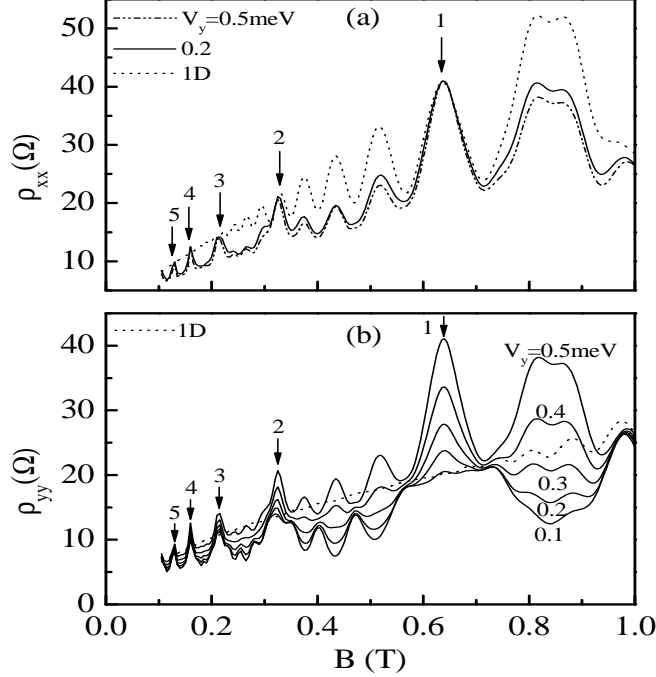


FIG. 6: Resistivity components ρ_{xx} and ρ_{yy} as a function of the magnetic field B for fixed $V_x = 0.5$ meV and varying V_y . The dotted curve is the 1D limit obtained with $V_y = 0$. The prominent peaks in the 2D case are marked by the integral value of $\alpha = \Phi_0/\Phi$.

ductivity. The smaller peaks, between these values of α , correspond to the commensurability or Weiss oscillations. Notice how the prominent peaks of ρ_{xx} , in the 2D case, remain rather insensitive to changes in V_y : this is so because they result from the collisional contribution σ_{yy}^{col} which depends very weakly on V_y through the energy spectrum. The apparently drastic difference between the two figures results from the fact that $\sigma_{\mu\mu} \ll \sigma_{xy}$ makes S change little and $\rho_{xx} = \sigma_{yy}/S$ while $\rho_{yy} = \sigma_{xx}/S$. Upon reducing V_y the contribution $\sigma_{xx}^{dif} \sim V_y^2$, given by Eq. (18), is affected drastically whereas σ_{yy}^{col} is not.

In Figs. 4 and 5 we plot again ρ_{xx} and ρ_{yy} as function of the field B with $V_x = V_y = 0.5$ meV, for the same τ and $\Gamma \propto B^{1/2}$ as in Fig. 6 but with the period a_y being doubled from panel to panel as indicated. The solid curves give the total resistivity, the dashed ones the diffusive contribution, defined by $\rho_{\mu\mu}^{dif} = \sigma_{\nu\nu}^{dif}/S$, and the dotted ones the collisional contribution, defined by $\rho_{\mu\mu}^{col} = \sigma_{\nu\nu}^{col}/S$. Notice how the prominent peaks move to lower fields with increasing a_y as explained after Eq. (26); in panel (d) they have disappeared. The 1D limit shown in panel (d) is obtained with $V_y = 0$ and the difference in the B dependence

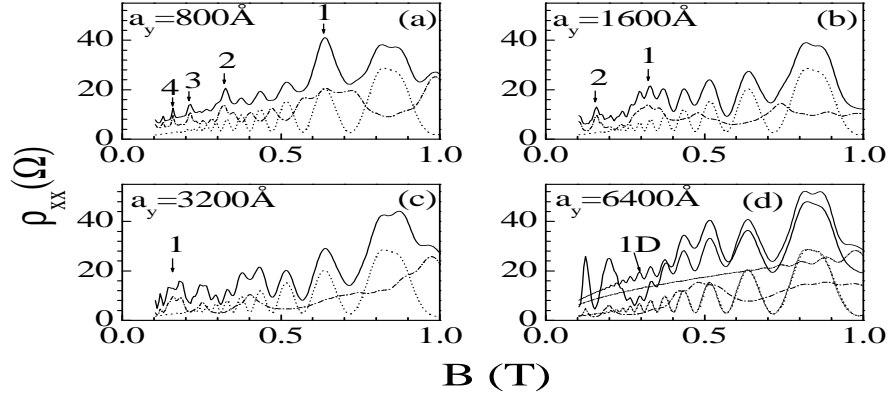


FIG. 7: Resistivity component ρ_{xx} as a function of the magnetic field B for fixed $V_x = V_y = 0.5$ meV and different periods a_y as indicated. The solid curves give the total resistivity, the dotted ones the diffusive contribution, and the dash-dotted ones the collisional contribution. The thinner curves in panel (d) are for the 1D limit ($V_y = 0$.) The prominent peaks in the 2D case are marked by the integral values of α .

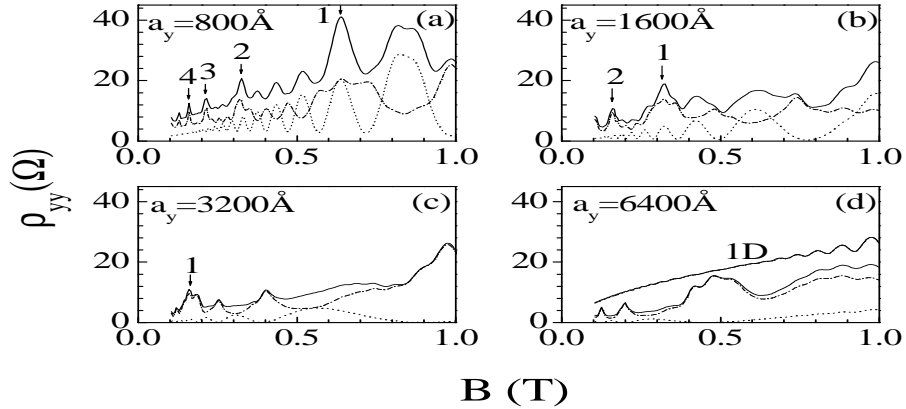


FIG. 8: The same as in Fig. 7 but for the resistivity component ρ_{yy} .

between ρ_{xx} and ρ_{yy} is related to that of the corresponding conductivity contributions. One of them, σ_{xx}^{dif} given Eq. (18), is affected drastically by changing V_y and/or the period a_y which enters the factor $\sin^2 \xi$, the others very weakly.

We now look more closely at the experimental results of Refs. 8 and 5 with the parameter sets specified above. The parameters V_x and V_y are not known. In Fig. 6 we have shown the total resistivity for $V_x = V_y = 0.5$ meV, constant $\tau = \tau_0$. In Fig. 9 we plot again ρ_{xx} versus B but now we show the contributions ρ_{xx}^{dif} and ρ_{xx}^{col} as well. In addition, we

take $V_x = V_y = 1$ meV, and $1/\tau \sim \Gamma \sim B^{1/2}$. Because $\sigma_{\nu\nu}^{dif} \ll \sigma_{\nu\nu}^{col}$, the difference in the total resistivity is very small between the two sets of modulation strengths. However, the oscillation amplitudes in $\rho_{\mu\mu}^{col}$ are higher in the present case and ρ_{xx} increases more slowly with B as observed [8]. Upon closer inspection we see that the prominent peaks, marked by the integral values of α , result entirely from the collisional contribution $\sigma_{\nu\nu}^{col}$. As can be seen in Fig. 3 of the next article [14], the amplitudes and positions of these peaks agree well to very well with the experimental results. Notice also how the Weiss oscillations of ρ_{xx}^{dif} and ρ_{xx}^{col} , between these peaks, are in antiphase. These experimental results for ρ_{yy} and ρ_{xx} are for two orthogonal crystal directions $[011]$ and $[01\bar{1}]$ taken from different samples. They have similar structures and the curves may be fitted theoretically using slightly different potentials. A direct comparison between experimental and theoretical results is made in Fig. 9 of the next article [14] for $\tau = \tau_0$ but qualitatively the agreement is the same for $\tau \propto B^{-1/2}$. Notice, however, that the theoretical oscillation amplitudes and the overall value of ρ_{xx} in the low- B region, below $\alpha = 2$, agree less well with the experimental ones than those in the high- B region.

In Ref. [14] results are given for temperature 1.6 K and otherwise the same parameters. We show the calculated ρ_{xx} for this case in Fig. 10. As can be seen, lowering the temperature makes visible all prominent peaks marked by arrows for $\alpha = 1, \dots, 8$. Their positions occur at fields $B = 0.64, 0.32, 0.21, 0.16, 0.13, 0.11, 0.09, 0.08$ T and compare very well with the experimental ones, see Fig. 6 in the next article [14]. To see more clearly the oscillations we replot, in Fig. 11, the resistivities in the low-field region of Fig. 10 as a function of $1/B$.

The temperature dependence of the oscillations is shown in Fig. 12. The solid, dotted, and thin solid curves correspond to $T = 5, 10, 20$ K, respectively. As can be seen, these new oscillations are more robust than the Weiss oscillations and persist at $T = 20$ K. However, their damping with T is weaker than the observed one [14].

In Fig. 13 we plot ρ_{xx} in the manner of Fig. 9 but for the parameters of Ref. 5 involving the much longer periods $a_x = a_y = 2820$ Å. The modulation strengths are $V_x = V_y = 0.2$ meV and very close to those used in Refs. 5 and 6. The agreement with the experimental 2D results of Ref. 5 is very good: below approximately $B = 0.5$ T we have the Weiss oscillations and above it the Shubnikov-de Haas ones. One noticeable feature here is the absence of the prominent peaks for integral values of α . This is so because the much longer periods involved make $\alpha = 2\pi\ell^2/a_x a_y$ integer for much smaller values of B . For instance,

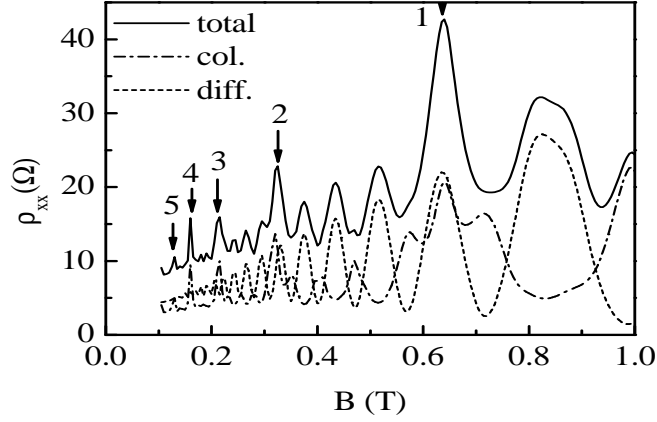


FIG. 9: Resistivity component ρ_{xx} as a function of the magnetic field B for fixed $V_x = V_y = 1$ meV and $T = 5.5$ K. The solid curves give the total resistivity, the dotted ones the diffusive contribution, and the dash-dotted ones the collisional contribution. The prominent peaks are marked by the integral values of $\alpha = \Phi_0/\Phi$.

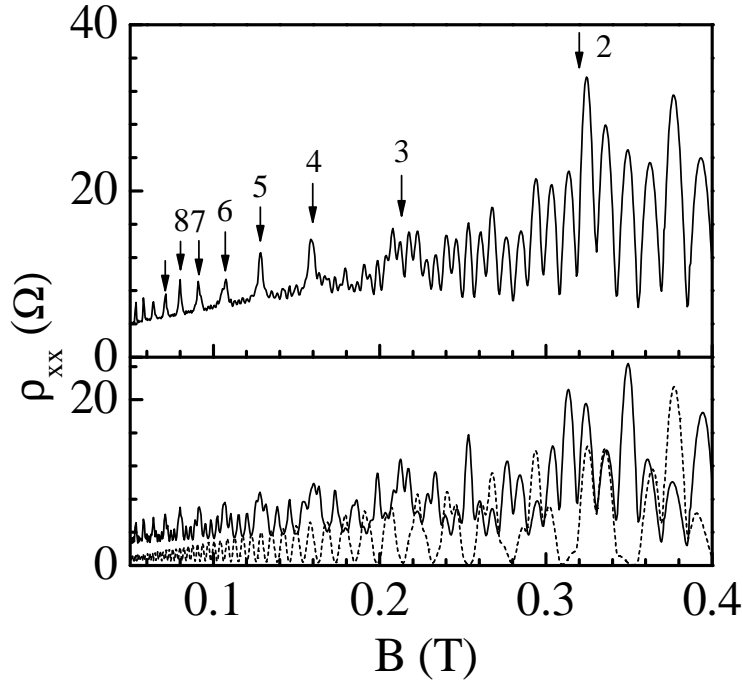


FIG. 10: The same as in Fig. 9 but for temperature $T = 1.6$. The lower panel shows the collisional contribution (solid curve) and the diffusive one (dotted curve); the upper panel shows their sum.

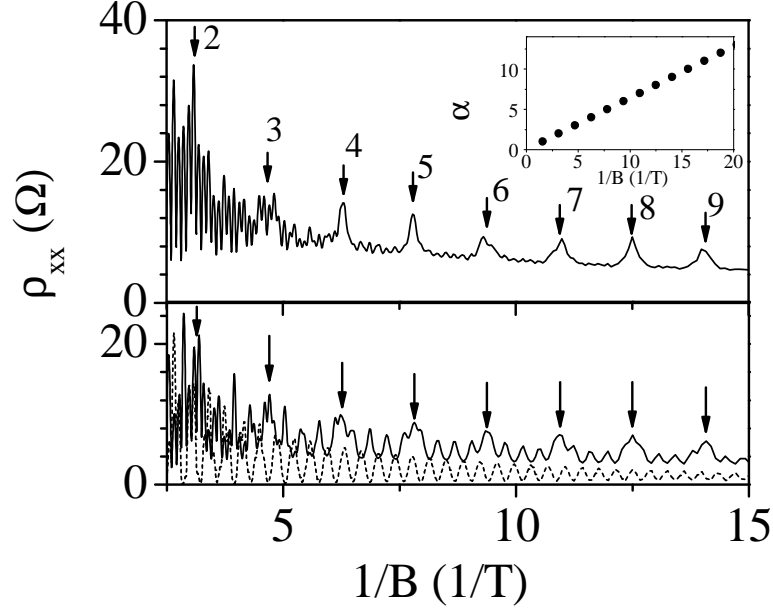


FIG. 11: Resistivity component ρ_{xx} as a function of inverse magnetic field $1/B$. The curves are marked as in Fig. 10. The inset shows the peak position versus $1/B$.

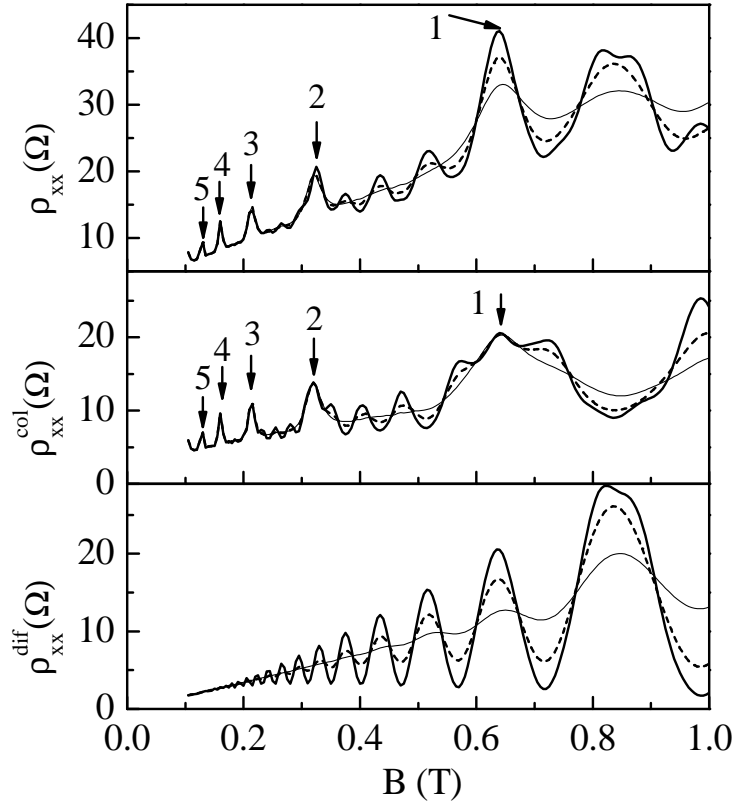


FIG. 12: Resistivity component ρ_{xx} as a function of the magnetic field B . The solid, dotted, and thin solid curves correspond to $T = 5, 10, 20$ K, respectively.

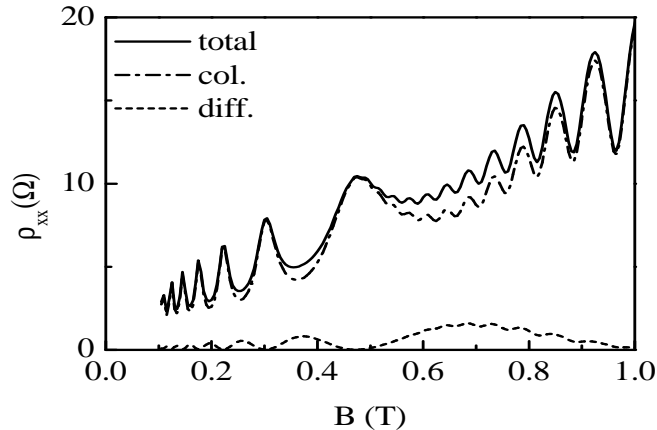


FIG. 13: The same as in Fig. 9 with the parameters of Ref. 5 and $V_x = V_y = 0.2$ meV.

$\alpha = 1$ occurs at $B = 0.05$ T and the corresponding peak is not resolved. The agreement is also as good if we use $a_x = a_y = 3650$ Å and otherwise the same parameters pertaining to another sample.

Reference 5 reported results also for 1D modulations. As mentioned earlier, we can obtain the 1D limit from the present 2D results by considering a vanishing V_y . In Fig. 14 we show the 1D limit of the total ρ_{xx} and ρ_{yy} for $a_x = 2820$ Å, $V_x = 0.5$ meV, and $V_y = 0$. Although the agreement between theory and experiment is very good, it must be noticed that it is obtained with $V_x = 0.5$ meV and not $V_x = 0.2$ meV that we used in Fig. 13. Since the 1D or 2D modulations are produced by illumination of the samples, we expect them to have the same strength. If we use $V_x = 0.2$ meV we can obtain good agreement if we use a τ smaller by about a factor of 2 in Eq. (18). As stated in Refs. 5 and 6, this may be an indication that in this very high mobility samples the fine structure of the energy spectrum, that the present theory neglects, is partially resolved. However, the experimental data was taken at $T = 4.2$ K and, as no such fine structure has been observed above mK temperatures, alternative explanations have been proposed [4], [14].

Finally, in Fig. 15 we show the Hall resistivity ρ_{yx} for the parameters of Fig. 9. As in the case of 1D modulations, it exhibits very weak oscillations. They are better seen in the inset which shows the derivative $d\rho_{yx}/dB$ versus B . The triangles on the x axis mark the positions of the integral values of α for which enhanced oscillations are observed.

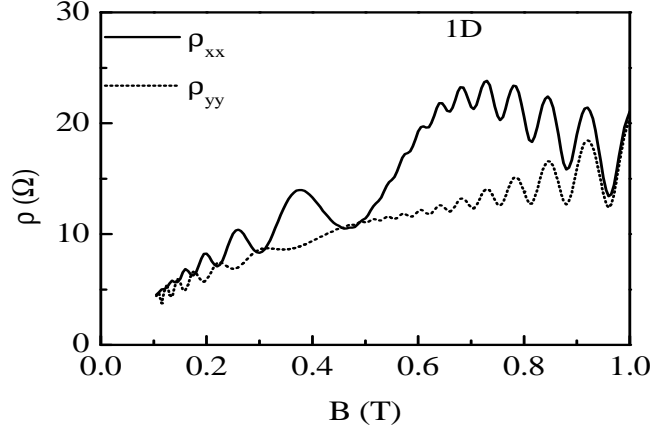


FIG. 14: The 1D resistivity component $\rho_{\mu\mu}$ as a function of the magnetic field B obtained with $a_x = 2820 \text{ \AA}$, $V_x = 0.5 \text{ meV}$, and $V_y = 0$.

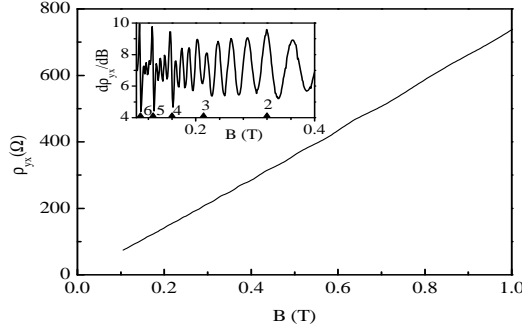


FIG. 15: The Hall resistivity ρ_{yx} versus magnetic field B with the parameters of Fig. 9. The inset shows the derivative $d\rho_{yx}/dB$ versus B .

V. CONCLUDING REMARKS

We presented a theory of magnetotransport in 2D superlattices using the energy spectrum and wave functions that result from the tight-binding difference equation when the parameter $\alpha = \Phi_0/\Phi$ is an integer. As emphasized in the text and supported with the results for the DOS shown in Fig. 4, the description holds approximately for all fields if we assume that the small gaps in the energy spectrum are closed due to disorder. The reasonable-to-good agreement with the experimental results strongly supports this assumption.

As detailed in the text, the prominent peaks, for $\alpha = \Phi_0/\Phi$ integer, result from the

collisional contribution to the conductivity σ_{yy}^{col} , require sufficiently *short* periods, and depend very weakly on the value of the modulation strengths V_x and V_y . Upon increasing the period along one direction we showed how they move to lower fields. Accordingly, for periods between 3000 Å and 4000 Å these peaks occur at much smaller magnetic fields and are not resolved [5]. The agreement between our results and the experimental ones, as presented in Ref. 8 and detailed in the next article [14], is good for the peak positions at all fields. The oscillation amplitudes agree well at relatively high fields but less well at low fields. As shown in Fig. 12, these oscillations are quite robust with respect to the temperature but their damping with temperature is weaker than the observed one.

Between the oscillations for $\alpha = \Phi_0/\Phi$ integer we have the Weiss oscillations. The relative phase between those of ρ_{xx} and those of ρ_{yy} depends on the values of the modulation strengths, cf. Fig. 6 in which the period is the same for all curves, and of the modulation periods, cf. Figs. 4 and 5 in which the modulation strengths are the same for all panels. We notice that as V_y becomes smaller and smaller than V_x , the oscillations resemble more closely those corresponding to 1D *weak* modulations [15], cf. Fig. 6. The results for the latter can be extracted from the present 2D ones if we take the modulation strength along one direction to be zero.

The relative phase between ρ_{xx} and ρ_{yy} for 1D and 2D modulations depends strongly on the ratio of the modulation strengths V_x and V_y . Since one resistivity component vanishes for 1D modulations, this conclusion could not be reached by studying only the latter. Similar results were reported in Ref. 6.

Acknowledgments

This work was supported by the Canadian NSERC Grant No. OGP0121756, the Belgian Interuniversity Attraction Poles (IUAP), the Flemish Concerted Action (GOA) Programme, and the EU-CERION programme. We also thank A. Long and J. H. Davies for stimulating discussions and important clarifications concerning the experimental results of the next article.

-
- [1] D. Weiss, K. von Klitzing, K. Plog, and G. Weimann, Europhys. Lett. **8**, 179 (1989); R. W. Winkler, J.P. Kotthaus, and K. Ploog, Phys. Rev. Lett. **62**, 1177 (1989).

- [2] R. R. Gerhardts, D. Weiss, and K. von Klitzing, *Phys. Rev. Lett.* **62**, 1173 (1989); C. W. J. Beenakker, *ibid* **62**, 2020 (1989); P. Vasilopoulos and F. M. Peeters, *ibid* **63**, 2120 (1989); H. L. Cui, V. Fessatidis, and N. Horing, *ibid* **63**, 2598 (1989); P. Streda and A.H. MacDonald, *Phys. Rev. B* **41**, 11892 (1990); C. Zhang and R. R. Gerhardts, *ibid* **41**, 12850 (1990); F. M. Peeters and P. Vasilopoulos, *ibid* **42**, 5899 (1990).
- [3] F. M. Peeters and P. Vasilopoulos, *Phys. Rev. B* **46**, 4667 (1992).
- [4] D. E. Grant, A. R. Long, and J. H. Davies, *Phys. Rev. B* **61**, 13127 (2000); F. M. Peeters and P. Vasilopoulos, *Proceedings of the 20th International Conference on the Physics of Semiconductors*, edited by E. M. Anastassakis and J. D. Joannopoulos (World Scientific, Singapore, 1990), Vol. 2, p. 1589.
- [5] R. R. Gerhardts, D. Weiss, and U. Wulf, *Phys. Rev. B* **43**, 5192(1991).
- [6] D. Pfannkuche and R. R. Gerhardts, *Phys. Rev. B* **46**, 12606 (1992).
- [7] E. S. Alves, P. H. Beton, M. Henini, L. Eaves, P. C. Main, O. H. Hughes, G. A. Toombs, S. P. Beaumont, C. D. W. Wilkinson, *J. Phys.: Cond. Matter* **1**, 8257 (1989); H. Fang and P. J. Stiles, *Phys. Rev. B* **41**, 10171 (1990); A. Toriumi, K. Ismail, M. Burkhardt, D. A. Antoniadis, and Henry I. Smith, *Phys. Rev. B* **41**, 12346 (1990).
- [8] S. Chowdhury, A. R. Long, J. H. Davies, K. Lister, and E. Skuras, EP2DS-14.
- [9] S. Chowdhury, C. J. Emeleus, B. Milton, E. Skuras, A. R. Long, J. H. Davies, G. Pennelli, and C. R. Stanley, *Phys. Rev. B* **62**, R4821 (2000); P. Rotter, M. Suhrke, and U. Rössler, *ibid*, **54**, 4452 (1996); C. Albrecht, J. H. Smet, D. Weiss, K. von Klitzing, R. Hennig, M. Suhrke, U. Rossler, V. Umansky, and H. Schweizer, *Phys. Rev. Lett.* **86**, 147 (2001).
- [10] J. Labbé, *Phys. Rev. B* **35**, 1373 (1987).
- [11] D. R. Hofstadter, *Phys. Rev. B* **14**, 2239 (1976); F. H. Claro and G. H. Wannier, *Phys. Rev. B* **19**, 6068 (1979).
- [12] N. A. Usov, *Zh. Eksp. teor. Fiz.* [Sov. Phys. JETP **67**, 2565 (1988)].
- [13] P. Vasilopoulos and C.M. Van Vliet, *J. Math. Phys.* **25**, 1391 (1984); *Phys. Rev. B* **34**, 4375 (1986); P. Vasilopoulos, *ibid* **32**, 771 (1985); *ibid* **34**, 3019 (1986).
- [14] S. Chowdhury, A. R. Long, J. H. Davies,.....
- [15] For recent studies of *strong* 1D modulations and the relevant observations or predictions, we refer the reader to the following works: J. Shi, F. M. Peeters, K. W. Edmonds, and B. L. Gallagher, *Phys. Rev. B* **66**, 035328 (2002); M. Langenbuch, M. Suhrke, and U. Rössler,

Europhys. Lett. **61**, 520 (2003); K. Vyborny, L. Smrcka, and R. A. Deutschmann, Phys. Rev. B **66**, 205318 (2002).